The 8th International Conference on Jets, Wakes and Separated Flows, ICJWSF-2024
September 23-25, 2024, Firenze, Italy

Experimental analysis of boundary condition effects on the pressure field within an RDC

Hongyi Wei [1*], Eric Bach[2], Christian Oliver Paschereit[1] and Myles D. Bohon[1]

1: Chair of Pressure Gain Combustion,Technische Universität Berlin, Germany
2: School of Mechanical Engineering, Purdue University, USA

[*] Corresponding author: hongyi.wei@tu-berlin.de

Abstract

The pressure field inside the rotating detonation combustor (RDC) exhibits significant complexity. In this study, eleven piezoelectric sensors were mounted to measure a synchronized, two dimensional pressure field around the combustor. Two distinct outlet boundary configurations — blunt plates and a set of nozzle guide vanes (NGVs) - were tested to investigate their effects on the pressure field, with findings compared to simulations derived from a two-dimensional fast reactive Euler solver. The results indicate that, for the configurations employing uniform outlet plates, the oblique shock angle decreases as the amount of outlet blockage increases, while the intensity of the outlet reflections amplifies consistently with heightened outlet restrictions. The pressure field map constructed from experimental data shows a good agreement with the simulations from the 2D solver. Furthermore, the integration of NGVs significantly mitigates the outlet reflection.

Keyword: *RDC, pressure field, NGVs*

Nomenclature

Symbols

A	=	area
$\dot{m}$	=	mass flow rate
p	=	pressure
f	=	frequency
s	=	speed
α	=	oblique shock angle
β	=	outlet reflection angle

Station Numbers

3.1	=	air injection area
3.2	=	combustion annulus
8	=	outlet throat

1. Introduction

Rotating detonation combustion (RDC) is a novel technique in the pressure gain combustion family, promising to further improve thermal efficiency. Understanding the circumferential structure of the dynamic flow field inside an RDC is crucial for grasping the nature of its pressure gain. This task is complex, involving coupled influences of physical boundary conditions, local mixture variations, and operating modes [1, 2]. Few studies have detailed the connection between the pressure profile inside the combustor and phenomena occurring within the RDC. Additionally, instantaneous pressure measurements struggle to reveal representative features of the pressure profile due to the highly unsteady environment inside the RDC. To complicate

matters, one potential application of RDCs is integration with turbines [3], where the high enthalpy outflow interacts with turbine blades, altering the flow field upstream inside the RDC.

In previous work, Wei et al. [4] identified key features of the pressure field inside the RDC, such as the oblique shock and the outlet reflection, through phase-averaged pressure analysis. However, with only four sensor pairs positioned along the combustion section, the study provided limited insight into the shock wave interactions with the outlet boundaries. To address this limitation, the present study aims to construct a higher-resolution pressure field map extending from the detonation region to the combustor exit, offering a detailed view of the complex flow field along the RDC's axial direction. The study will experimentally validate the pressure features identified by Wei et al. [4] and compare them with simulation results from a 2D fast reactive Euler solver developed by Klopsch et al. [5]. Additionally, it will investigate the impact of discrete outlet boundaries on RDC performance by comparing uniform outlet restrictions under different operating conditions, thereby supporting RDC applications for turbine integration.

2. Experimental setup

Figure 1 depicts the RDC setup at TU Berlin. The outer body of the RDC has a total length of 190 mm, comprising a 110 mm combustion section and an 80 mm vane section. The combustor's diameter is 90 mm, with a 7.6 mm annulus width where the detonation wave propagates. As indicated by blue arrows in the figure, air is injected into the combustor through a 1 mm annular slot and mixed with hydrogen in a jet-in-cross-flow configuration. Hydrogen is injected via 100 holes each 0.5 mm in diameter, represented by red arrows. An air mass flow rate of 350 g/s and a stochoimetric condition are targeted to achieve a clear single-wave mode.

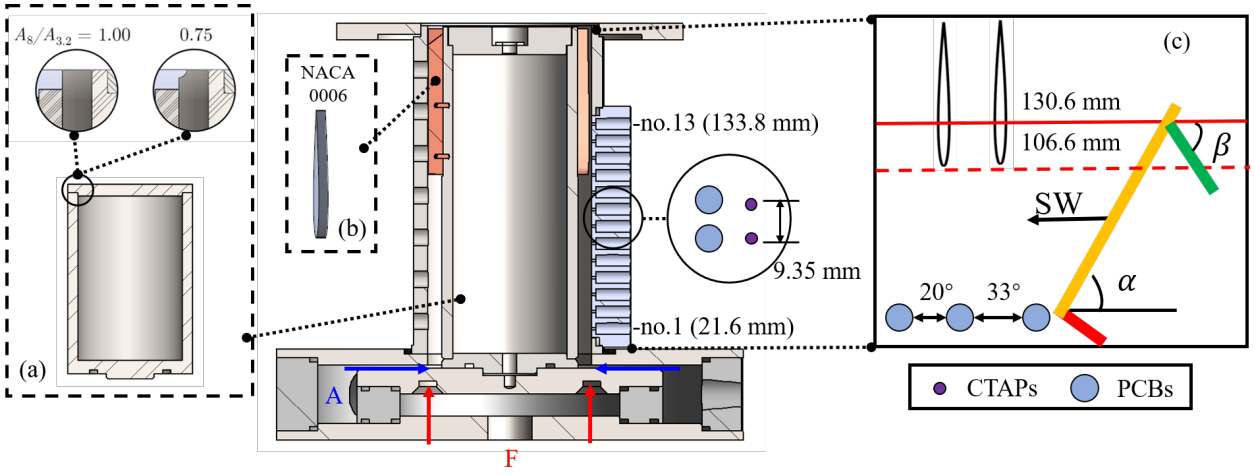

Fig. 1: Cross section of TU Berlin's RDC with nozzle guide vanes installed.

In this study, two types of outlet boundaries are tested. The first type consists of outlet plates with tips that protrude into the annulus, creating 0%, 16%, 25%, and 33% outlet blockages at the combustor exit, as depicted in Fig.1(a). The second type involves nozzle guide vanes (NGVs), which introduce blockages of 11%, and 16% by installing 6, and 9 vanes, respectively, as shown in Fig.1(b). Using the upper surface of the fuel plate as a reference (0 mm), the leading edge and the maximum cross-section of the NGVs are located at 106.6 mm and 130.6 mm, respectively. The operating conditions are summarized in Tab.1.

As illustrated in Figure 1, to investigate the pressure field from near the detonation front up to the leading edge of the NGVs, a custom-designed sensor block is employed. This block accommodates thirteen pairs of sensors along the combustor's axial direction, with only the first eleven ports utilized in this study. Each axial location houses one CTAP for static pressure measurements and one PCB for dynamic pressure measurements. The first sensor pair is positioned 21.6 mm from the reference surface, while the last pair is 133.8 mm away. Additionally, three more PCB sensors are mounted at the same axial location (25.6 mm) but at different azimuthal positions to aid in identifying the operating mode. To prolong the sensor survival time, the run time is limited to 300 ms. Data acquisition is performed at a sampling rate of 500 kHz.

Tab. 1: Range of varied parameters

Parameter	Value
$\dot{m}$	350 g/s
$A_{3:1}/A_{3:2}$	0.144
$A_8/A_{3:2}$ (blunt plates)	[1; 0.84; 0.75; 0.67]
$A_8/A_{3:2}$ (NGVs)	[0.89; 0.84]

Tab. 2: Flow field parameters

No.	$A_8/A_{3:2}$,[-]	f,Hz	s,m/s	α,	β,	$p_{peak;11}$,bar
1	1	6099.8	1724.7	53.5	9.6	0.51
2	0.84	6179.8	1747.3	51.5	14.6	0.70
3	0.75	6139.8	1736.0	49.1	17.6	0.81
4	0.67	5999.8	1696.4	54.5	20.0	1.01

3. Results and discussion

In this study, the pressure components within the RDC pressure field identified by Wei et al. [4] will be validated using a higher sensor density. A detailed pressure field map will be constructed for varying outlet restrictions provided by blunt plates, and the results will be compared with simulations from a 2D fast reactive Euler solver. Finally, the impact of NGVs, serving as turbine proxies, on the pressure field will be analyzed to explore their implications for RDC applications.

3.1. Pressure field influenced by uniform outlet plates

The pressure field inside the RDC is highly complex due to the interactions between the detonation wave, oblique shock wave, and boundary conditions. The presence of multiple co-/counter-rotating waves within the combustor further complicates the understanding of the circumferential pressure field structure. To simplify this challenge, we focused on single-wave mode cases, which exhibit clear propagation behavior, thereby reducing the difficulty in identifying the pressure components.

Given the highly unsteady nature of the RDC, the cycle-to-cycle pressure profile exhibits stochastic behavior. Therefore, phase-averaged pressure is useful for revealing a representative pressure trace. To achieve this, the final 50 ms of dynamic pressure data measured by the PCB sensors was selected and divided into 200 time windows. Each window captures three neighboring detonation laps, enhancing the visualization of pressure component propagation. The phase-averaged pressure was then calculated using the Euclidean mean method.

Figure 2 presents the phase-averaged pressure profiles obtained from eleven PCB sensors along the combustor's axial direction under varying outlet restrictions provided by blunt plates, with 0%, 16%, 25%, and 33% blockages at the combustor exit. Due to the space limit, a section corresponding to 1.5π to 4.5π of the three detonation laps is displayed. The relevant flow field parameters are provided in Tab. 2.

Building on the research by Wei et al. [4], the highest peak in the phase-averaged pressure during one detonation lap in Fig.2 is identified as the combined detonation wave and oblique shock wave, which propagates from upstream to downstream across the full axial length of the combustor. Due to the limited response time of the pressure sensors, the pressure peak is not a reliable indicator for determining the exact timing when the detonation wave/oblique shock wave passes. Instead, the maximum gradient of the pressure trace is used to define the onset of this phenomenon, as indicated by the red circles in Fig.2. The oblique shock angle is then calculated using linear polynomial regression of these red markers. As shown in Tab.2, the calculated oblique shock angle decreases from 53.5° to 49.1° as the outlet restriction increases from $A_8/A_{3:2} = 1$ to $A_8/A_{3:2} = 0.75$, consistent with the findings of Klopsch et al. [5].

As the oblique shock wave propagates from upstream to downstream and interacts with the outlet boundary, it generates an outlet reflection [4]. This reflection, occurring near 105.75 mm as shown in Fig.2, then propagates back upstream, with its path marked in green in the figure. Comparing the propagation path of this

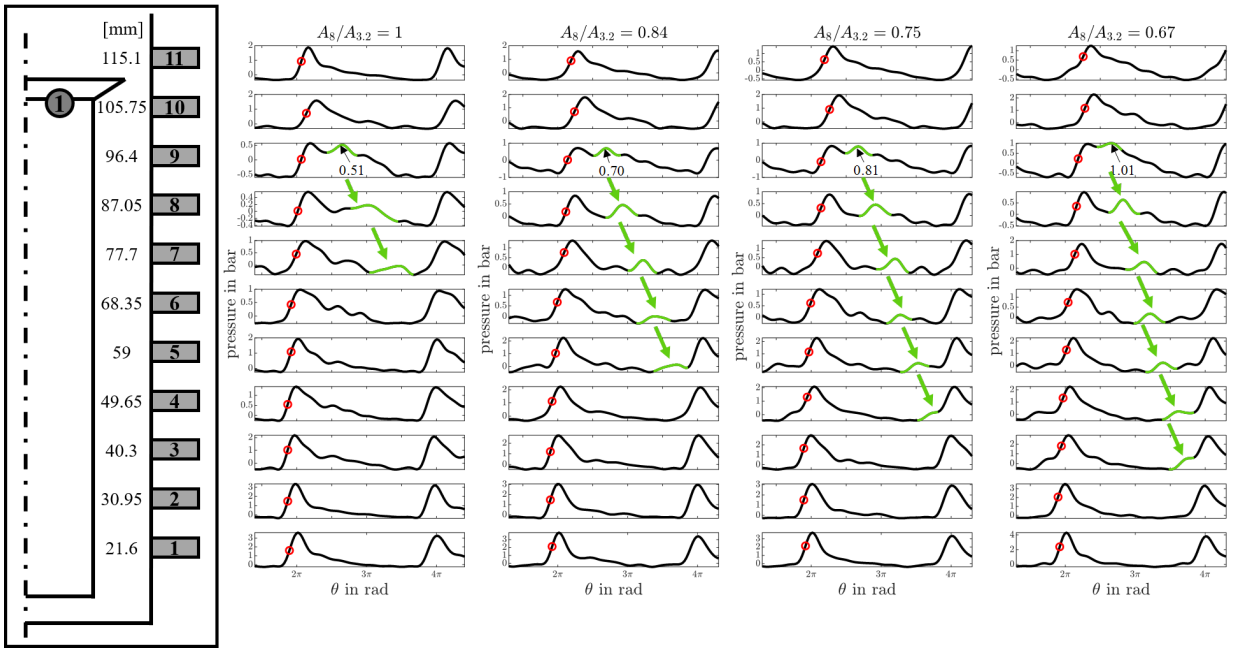

Fig. 2: Examples of phase-averaged pressure along the combustor axial direction for varying outlet restrictions.

pressure component for varying outlet restrictions, it can be seen that the more restricted outlet produces a stronger outlet reflection. For identical operating conditions but varying outlet restrictions, $A_8/A_{3:2} = 0.67$ produces the most pronounced outlet reflection, affecting the pressure field up to 40.3 mm upstream, whereas $A_8/A_{3:2} = 1$ influences the flow field only up to 77.7 mm. Additionally, the peak value of this pressure component at 96.4 mm increases with greater outlet restrictions, rising from 0.51 bar to 1.01 bar. The reflection angle β, detailed in Tab.2, exhibits the same trend, increasing from 9.6 to 20.0 with the increasing outlet restrictions.

3.2. Pressure field comparisons with 2D fast reactive Euler solver

Based on the phase-averaged pressure data presented in Fig.2, pressure field maps along the combustor's axial direction for varying outlet restrictions are constructed and displayed in Fig.3a, Fig.3c, Fig.3e, and Fig.3g. In these figures, each bright band represents the phase-averaged pressure measurements obtained from the PCB sensors, while the blue background indicates regions lacking measurement data. The color bars illustrate the amplitude of the pressure trace, scaled to enhance the visualization of the circumferential pressure field structure. The red solid and dashed lines denote the combustor exit and the exit throat, respectively, as defined by the outlet plates. Figures 3b, 3d, 3f, and 3h depict the pressure field simulated using a fast reactive Euler solver developed by Klopsch et al. [5]. Note that the simulations do not account for the pressure field behind the combustor, corresponding to the regions measured by sensor No. 11 in the experiments. The marker positions in the simulations are based on experimental results.

Figure 3a indicates that the detonation height is approximately 49.65 mm for $A_8/A_{3:2} = 1$ and decreases to 30.95 mm with increasing outlet restrictions. The pressure amplitude from the detonation wave/oblique shock wave diminishes beyond 59 mm but becomes more pronounced near the combustor exit at 105.75 mm. The simulated pressure contours in Fig.3b, Fig.3d, Fig.3f, and Fig.3h align well with the experimental results, particularly for the restricted cases, showing a deviation of only around 1 in the calculated oblique shock angle for $A_8/A_{3:2} = 0.67$.

3.3. Pressure field influenced by NGVs

To investigate the impact of discrete outlet boundaries on the pressure field, a set of nozzle guide vanes (NGVs) is used as a turbine proxy. Figure 4(a) shows the phase-averaged pressure for a configuration with 9 NGVs. Two installation positions of the NGVs relative to the sensor block are depicted by black and gray lines, representing misaligned and aligned configurations, respectively, as illustrated in Fig.4(b). It is

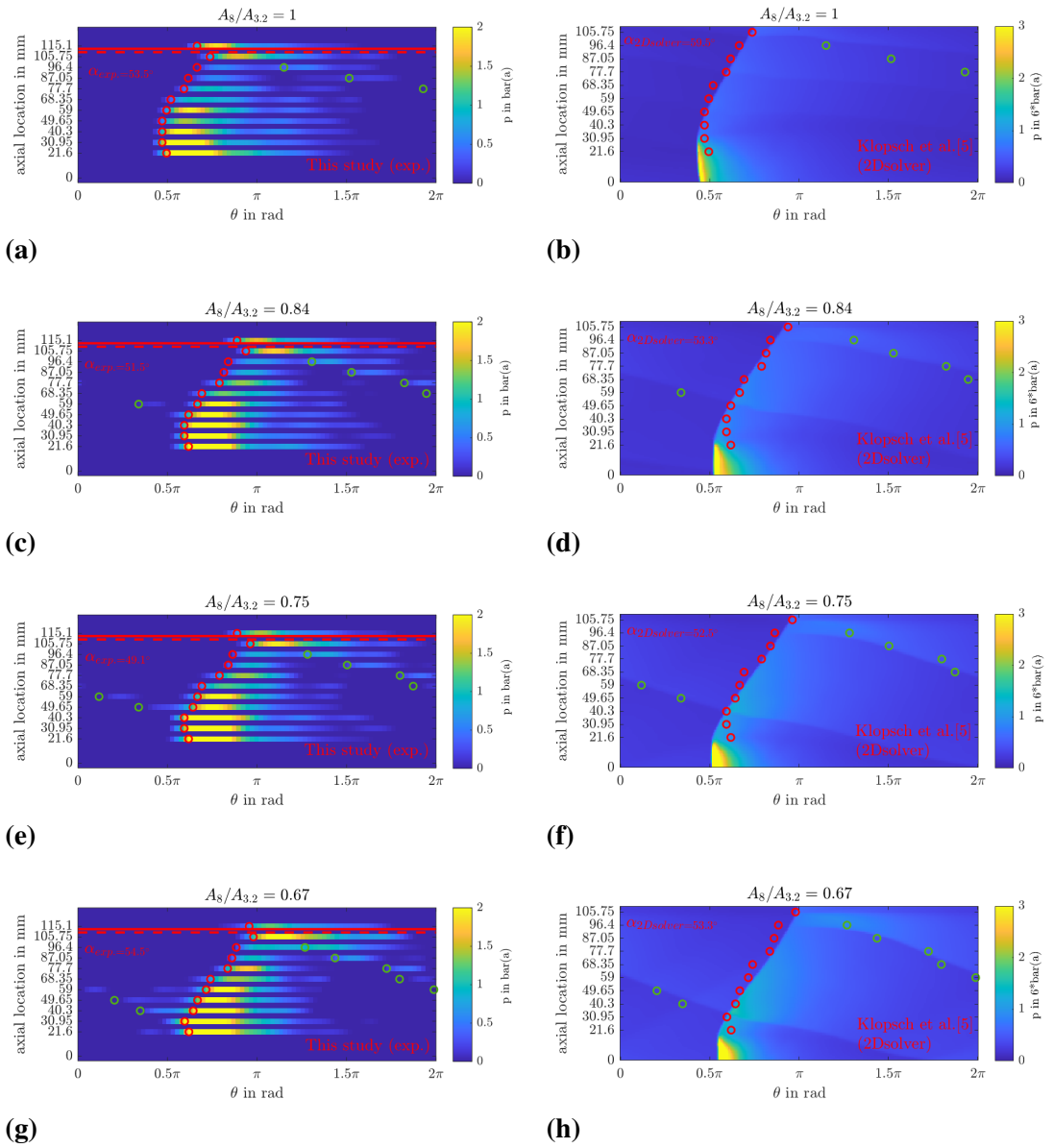

Fig. 3: Comparisons of pressure field maps constructed based on experimental data in this study (a)(c)(e)(g), and a 2D fast reactive Euler solver developed by [5] (b)(d)(f)(h).

evident from Fig.4(a) that these configurations do not affect the upstream pressure field but influence the regions where sensors No.10 and No.11 are located.

Figure 4(c) presents the pressure field map with 9 NGVs installed in a misaligned configuration, where the red dashed line and solid line denote the leading edge and the maximum cross-section of the NGVs, respectively. Compared to Fig.3c, the outlet reflection (indicated in green) is significantly reduced and does not affect the pressure field very far upstream, such as at 59 mm. This observation is consistent with findings from our previous study [4], which demonstrated that NGVs effectively diminish outlet reflection. As a result of the weaker outlet reflection, the oblique shock angle is 3 higher than that observed in Fig.3c, which aligns with our expectation that reduced outlet reflection corresponds to an increased oblique shock angle, as discussed in section 3.1. Additionally, gas products pass through the gap between the two neighboring NGVs, resulting in a noticeable time delay between the pressure measurements from sensors No.10 and No.11, as shown in Fig.4(c).